ON THE POTENTIAL OF SPATIALLY-SPREAD ORTHOGONAL TIME FREQUENCY SPACE MODULATION FOR ISAC TRANSMISSIONS

Shuangyang Li[⋆]*, Weijie Yuan*[†]*, Jinhong Yuan*[⋆]*, and Giuseppe Caire*[‡]

[⋆]University of New South Wales, Sydney, Australia
[†]Southern University of Science and Technology, Shenzhen, China
[‡]Technische Universität Berlin, 10587 Berlin, Germany
(*Invited Paper*)

ABSTRACT

In this paper, we study the potentials of spatially-spread orthogonal time frequency space (SS-OTFS) modulation for integrated sensing and communication (ISAC) transmissions. The most favourable feature of SS-OTFS modulation is that it forms beams according to a pre-determined angular grid, which is different from the conventional beamforming, where dedicated beams are formed according to the *a priori* information on the angle of departures (AoDs). According to the delay-Doppler domain channel characteristics, we first derive the input-output relationships for SS-OTFS-enabled ISAC system in a typical downlink multi-user MIMO (MU-MIMO) scenario. Based on those relationships, we further study the angular domain channel features and discuss the system design. Our numerical results have demonstrated the advantages of the proposed scheme over the conventional beamforming counterpart in terms of the signal-to-interference-plus-noise ratio (SINR).

***Index Terms*—** ISAC, spatially-spread, OTFS

1. INTRODUCTION

Integrated sensing and communication (ISAC) transmission has been widely recognized as an efficient approach to deal with the foreseeable coexistence between communication and radar [1, 2, 3]. In particular, ISAC transmissions allow effective cooperations between communication and radar sensing functionalities and have shown great potentials in improving both the performances of communication and radar sensing [4]. For the design of ISAC transmissions, it is worthwhile to notice that radar sensing carries out parameter estimation based on the delay, Doppler, and angular features associated to resolvable paths, whose core idea aligns perfectly with the recently proposed orthogonal time frequency space (OTFS) modulation [5, 6]. Specifically, OTFS modulation relies on the exploration of the delay-Doppler (DD) domain symbol multiplexing based on the DD domain channel characteristics [7, 8], which can be potentially inferred from the sensing estimates in practice [2].

Many research works have considered OTFS-based ISAC transmissions [9, 10, 11]. For example, the effectiveness of OTFS modulation for ISAC transmission has been evaluated in [10], where the authors have demonstrated that the estimation error lower bounds for radar sensing can be achieved by using OTFS signals while maintaining a satisfactory communication performance. This work has then been extended to the case of multiple-input multiple-output (MIMO) [11], where a hybrid digital-analog beamformer is devised for both radar sensing and communication. Although the applications of OTFS modulation in ISAC transmissions have shown promising performances, they often rely on beamforming schemes [2, 11, 12] that are designed according to the *a priori* information on the angle of departures (AoDs). However, conventional beamforming suffers from significant inter-beam interference when different beams have close angular features, and is very sensitive to estimation errors on AoDs.

Considering the potential issue of beamforming, we investigate on the potentials of spatially-spread OTFS (SS-OTFS) modulation [13] for ISAC transmissions in a typical downlink multi-user MIMO (MU-MIMO) scenario. Different from conventional MIMO-OTFS modulation, SS-OTFS applies the so-called "spatial spreading" and "spatial de-spreading" modules at the transmitter and receiver, respectively. The key novelty of applying those modules is the **discretization** of the angular domain, where the beams are formed according to a pre-defined angular grid. Consequently, such a scheme is shown to be robust to the estimation errors on AoDs. In this paper, we first derive the vector representations of the input-output relationships for both functionalities. Based on those relationships, we investigate on the angular domain channel characteristics and briefly discuss the design of SS-OTFS-enabled ISAC transmissions. We present the numerical results on the signal-to-interference-plus-noise (SINR) for both communication and radar, where we show that SS-OTFS-enabled ISAC transmission enjoys better SINR performances for both communication and radar compared to the beamforming counterpart.

Notations: The blackboard bold letters $\mathbb{A}$, $\mathbb{C}$, and $\mathbb{E}$ denote the energy-normalized constellation set, the complex number field, and the expectation operator, respectively; $\mathrm{vec}(\cdot)$, "$\otimes$", and $[\cdot]_N$ denote the vectorization, the Kronecker product, and the modulo-N operators, respectively. $\mathbf{F}_N$, $\mathbf{I}_N$, and $\mathbf{0}_N$ denote the discrete Fourier transform (DFT) matrix, the identity matrix, and an all-zero matrix of size $N \times N$, respectively.

2. SYSTEM MODEL

Consider an ISAC system serving K randomly distributed user equipments (UEs), where a mono-static radar with co-located transmitter and receiver is equipped at the base station (BS). We are interested in a typical MU-MIMO downlink scenario, where the BS equips N_{BS} antennas with $2K$ radio frequency (RF) chains in the form of a uniform linear array (ULA) while each UE has only one antenna. We assume that the system operates in an open

area, where there are P independent resolvable paths between the BS and each UE. Furthermore, we consider a general ISAC scenario, where the strongest channel responses for communication and radar sensing come from the first and second paths of each UE [1, 13][1]. Thus, the ISAC transmitter assigns two angular grid points for each UE based on the *a priori* information on AoDs via spatially-spreading, while applying spatially de-spreading at the radar receiver for further processing.

2.1. Equivalent Channel Matrices

Without loss of generality, we consider a reduced cyclic prefix (CP) signaling format with rectangular pulses for pulse shaping and matched-filtering. According to [14], the discrete time-delay-spatial (TDS) domain communication channel matrix with respect to the $n_{\rm t}$-th transmit antenna, for $1 \leq n_{\rm t} \leq N_{\rm BS}$, and the UE index i, for $1 \leq i \leq K$, can be modeled by

$$\begin{aligned}\mathbf{H}_{n_{\rm t},i}^{\rm TDS} &\triangleq \sum_{p=1}^{P} h_{i,p} \exp\left(j\pi\left(n_{\rm t}-1\right)\sin\varphi_{i,p}\right) \mathbf{\Pi}^{l_{i,p}} \mathbf{\Delta}^{k_i+\kappa_{i,p}} \\ &= \sum_{p=1}^{P} \exp\left(j\pi\left(n_{\rm t}-1\right)\sin\varphi_{i,p}\right) \mathbf{H}_{i,p}^{\rm TD}, \end{aligned} \tag{1}$$

where $\mathbf{H}_{i,p}^{\rm TD} \triangleq h_{i,p}\mathbf{\Pi}^{l_{i,p}}\mathbf{\Delta}^{k_{i,p}+\kappa_{i,p}}$ is defined as the time-delay (TD) domain communication channel matrix for the p-th path of the i-th UE. In (1), $h_{i,p}$, $\varphi_{i,p}$, $l_{i,p}$, $k_{i,p}$, and $\kappa_{i,p}$ are the communication fading coefficient, AoD, delay index, integer Doppler index, and fractional Doppler index associated to the p-th path of the i-th UE for communication, respectively. Meanwhile, $\mathbf{\Pi}$ and $\mathbf{\Delta}$ in (1) are the forward cyclic shift matrix of size $MN \times MN$ characterizing the delay influence and a diagonal matrix of the size $MN \times MN$ characterizing the Doppler influence, respectively. Unfortunately, we do not have enough space to give the definitions to the above parameters in this paper and we refer the readers to [14] for more details.

Similarly, the discrete TDS domain radar channel matrix with respect to the $n_{\rm t}$-th transmit antenna, $n_{\rm r}$-th receive antenna, for $1 \leq n_{\rm t}, n_{\rm r} \leq N_{\rm BS}$, and the UE index i, for $1 \leq i \leq K$, can be modeled by

$$\begin{aligned}\tilde{\mathbf{H}}_{n_{\rm t},i,n_{\rm r}}^{\rm TDS} &\triangleq \sum_{p=1}^{P} \tilde{h}_{i,p} \exp\left(j\pi\left(n_{\rm t}-1\right)\sin\varphi_{i,p}\right) \\ &\quad \exp\left(j\pi\left(n_{\rm r}-1\right)\sin\varphi_{i,p}\right) \mathbf{\Pi}^{\tilde{l}_{i,p}} \mathbf{\Delta}^{\tilde{k}_i+\tilde{\kappa}_{i,p}}, \\ &= \sum_{p=1}^{P} e^{j\pi(n_{\rm t}-1)\sin\varphi_{i,p}} e^{j\pi(n_{\rm r}-1)\sin\varphi_{i,p}} \tilde{\mathbf{H}}_{i,p}^{\rm TD}, \end{aligned} \tag{2}$$

where $\tilde{\mathbf{H}}_{i,p}^{\rm TD} \triangleq \tilde{h}_{i,p}\mathbf{\Pi}^{\tilde{l}_{i,p}}\mathbf{\Delta}^{\tilde{k}_i+\tilde{\kappa}_{i,p}}$ is the TDS domain equivalent radar channel matrix for the p-th path of the i-th UE. In (2), $\tilde{h}_{i,p}$, $\tilde{l}_{i,p}$, $\tilde{k}_{i,p}$, and $\tilde{\kappa}_{i,p}$ are the radar reflection coefficient, delay index, integer Doppler index, and fractional Doppler index associated to the p-th path of the i-th UE for radar sensing, respectively.

Remark 1: In practice, the radar reflection coefficient $\tilde{h}_{i,p}$ relates to the distance between the i-th UE and the BS with respect to the p-th path, the effective area of the radar receiving antenna, the RCS, the wavelength, and the transmit and receive antenna gains [15]. Therefore, $h_{i,p}$ and $\tilde{h}_{i,p}$ usually do not have the same value [1, 13].

[1]As indicated in the following sections, our proposed scheme can be easily applied to the case where the strongest channel responses for both communication and radar sensing are from the same path.

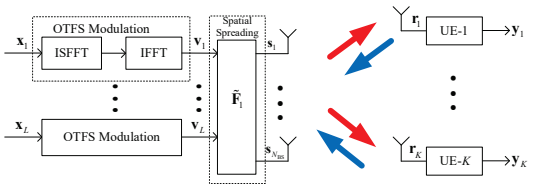

Fig. 1. A diagram of SS-OTFS-enabled ISAC transmission, where the red and blue arrows represent the transmitted signal and the received echo from the BS.

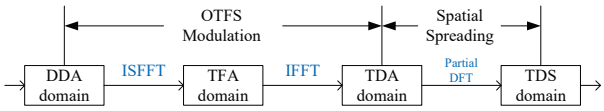

Fig. 2. The domain transformations the SS-OTFS enabled ISAC transmitter.

2.2. Transmitter Model

Without loss of generality, let us consider the SS-OTFS-enabled ISAC transmission diagram as shown in Fig. 1. Let M and N denote the number of orthogonal subcarriers and time slots, respectively. Furthermore, let $\{\mathbf{x}_1, \mathbf{x}_2, ..., \mathbf{x}_L\}$ be $L = 2K$ delay-Doppler-angular (DDA) domain data streams of length MN for the downlink transmission, where we intentionally repeat the transmit data stream *twice* for each UE in order to align the same data stream with the paths associated to the strongest channel responses for communication and radar sensing, e.g., $\mathbf{x}_i = \mathbf{x}_{i+K}$. Let $\mathbf{x} \triangleq \left[\mathbf{x}_1^{\rm H}, \mathbf{x}_2^{\rm H}, ..., \mathbf{x}_L^{\rm H}\right]^{\rm H}$ and $\mathbf{v} \triangleq \left[\mathbf{v}_1^{\rm H}, \mathbf{v}_2^{\rm H}, ..., \mathbf{v}_L^{\rm H}\right]^{\rm H}$ be the DDA domain and the time-delay-angular (TDA) domain information symbol vectors of length LMN, respectively. Then, we have $\mathbf{v} = \left(\mathbf{I}_L \otimes \mathbf{F}_N^{\rm H} \otimes \mathbf{I}_M\right)\mathbf{x}$ [14, 6]. The TDA domain information symbol vectors can be rearranged into a two-dimensional (2D) TDA domain information symbol matrix $\mathbf{V}$ of size $MN \times L$, whose i-th column is $\mathbf{v}_i$. Then, the TDS domain transmitted symbol matrix $\mathbf{S}$ of size $MN \times N_{\rm BS}$ is obtained by applying the *spatial spreading*, which can be implemented via a partial DFT matrix $\tilde{\mathbf{F}}_1$ of size $L \times N_{\rm BS}$. In particular, we have $\tilde{\mathbf{F}}_1 \triangleq \mathbf{P}_1\mathbf{F}_{N_{\rm BS}}^{\rm H}$, where $\mathbf{P}_1$ is a *transmit indicator matrix* of size $L \times N_{\rm BS}$ and is designed to assign the data stream to the desired angle similar to the idea of beamforming. As such, with a rectangular shaping pulse, the TDS domain transmitted symbols can be represented by

$$\mathbf{S} = \mathbf{V}\tilde{\mathbf{F}}_1 = \mathbf{V}\mathbf{P}_1\mathbf{F}_{N_{\rm BS}}^{\rm H}, \tag{3}$$

where the design of $\mathbf{P}_1$ will be discussed in the following section. Denote by $\mathbf{s}_{n_{\rm t}}$ the $n_{\rm t}$-th column of $\mathbf{S}$, and we have

$$\mathbf{s} \triangleq \left[\mathbf{s}_1^{\rm H}, \mathbf{s}_2^{\rm H}, ..., \mathbf{s}_{N_{\rm BS}}^{\rm H}\right]^{\rm H} = \left(\tilde{\mathbf{F}}_1^{\rm T} \otimes \mathbf{I}_{MN}\right)\mathbf{v}, \tag{4}$$

where $\mathbf{v} = \mathrm{vec}\left(\mathbf{V}\right)$. For a better understanding, we provide a diagram in Fig. 2, characterizing the domain transformations at the transmitter step by step. As shown in Fig. 2, the OTFS modulation transforms the data streams from the DDA domain to the

time-frequency-angular (TFA) domain and then to the TDA domain. After that, the partial DFT converts the signals from the TDA domain to the TDS domain for transmission.

2.3. Input-Output Relationships

According to (1), the TD domain[2] received symbol vector for the i-th UE is written by

$$\mathbf{r}_i = \sum_{n_{\rm t}=1}^{N_{\rm BS}} \mathbf{H}_{n_{\rm t},i}^{\rm TDS} \mathbf{s}_{n_{\rm t}} + \mathbf{q}_i = \sum_{p=1}^{P} \mathbf{H}_{i,p}^{\rm TD} \mathbf{V} \mathbf{P}_1 \mathbf{F}_{N_{\rm BS}}^{\rm H} \mathbf{a}\left(\varphi_{i,p}\right) + \mathbf{q}_i, \quad (5)$$

where $\mathbf{q}_i$ denotes the additive white Gaussian noise (AWGN) samples with one-sided power spectral density (PSD) N_0 and $\mathbf{a}\left(\varphi_{i,p}\right)$ is the transmit steering vector given by $\mathbf{a}\left(\varphi_{i,p}\right) \triangleq \frac{1}{\sqrt{N_{\rm BS}}}\left[1, e^{j\pi \sin\varphi_{i,p}}, ..., e^{j\pi(N_{\rm BS}-1)\sin\varphi_{i,p}}\right]^{\rm T}$. Then, by applying the conventional OTFS demodulation and after some mathematical derivations, the DD domain received symbol vector for the i-th UE is given by $\mathbf{y}_i = \left(\mathbf{F}_N \otimes \mathbf{I}_M\right)\mathbf{r}_i$.

Let $\tilde{N}_0$ denote the one-sided PSD for the radar noise, which takes into account of both the AWGN noise power from the channel and the interference power from the transmit signals after interference cancellation [1]. Similar to (5), the radar received TDS domain symbol vector for the $n_{\rm r}$-th antenna is written by

$$\tilde{\mathbf{r}}_{n_{\rm r}} = \sum_{i=1}^{K} \sum_{n_{\rm t}=1}^{N_{\rm BS}} \tilde{\mathbf{H}}_{n_{\rm t},i,n_{\rm r}}^{\rm TDS} \mathbf{s}_{n_{\rm t}} + \tilde{\mathbf{q}}_{n_{\rm r}}, \quad (6)$$

where $\tilde{\mathbf{q}}_{n_{\rm r}}$ denotes the TDS domain radar AWGN vector. Let $\tilde{\mathbf{R}} \in \mathbb{C}^{MN \times N_{\rm BS}}$ be the TDS domain received symbol matrix, whose $n_{\rm r}$-th column is $\tilde{\mathbf{r}}_{n_{\rm r}}$. After receiving $\tilde{\mathbf{R}}$, we apply the *spatial de-spreading*, i.e., the partial DFT matrix $\tilde{\mathbf{F}}_2 \triangleq \mathbf{F}_{N_{\rm BS}}\mathbf{P}_2$, where $\mathbf{P}_2$ is the *receive indicator matrix* designed to align the received signal to the corresponding RF chain. Thus, the resultant TDA domain received symbol matrix $\tilde{\mathbf{V}} \in \mathbb{C}^{MN \times L}$ can be written by

$$\tilde{\mathbf{V}} \triangleq \tilde{\mathbf{R}}\tilde{\mathbf{F}}_2 = \sum_{i=1}^{K}\sum_{p=1}^{P} \tilde{\mathbf{H}}_{i,p}^{\rm TD} \mathbf{V} \mathbf{P}_1 \mathbf{F}_{N_{\rm BS}}^{\rm H} \mathbf{A}\left(\varphi_{i,p}\right) \mathbf{F}_{N_{\rm BS}} \mathbf{P}_2 + \boldsymbol{\eta}, \quad (7)$$

where $\boldsymbol{\eta}$ denotes the TDS domain radar AWGN matrix with one-sided PSD $\tilde{N}_0$, and $\mathbf{A}\left(\varphi_{i,p}\right) \triangleq \mathbf{a}\left(\varphi_{i,p}\right)\mathbf{a}^{\rm T}\left(\varphi_{i,p}\right)$ is the steering matrix associated with the p-th path of the i-th UE.

3. ANGULAR DOMAIN CHANNEL CHARACTERISTICS AND SYSTEM DESIGN

For the p-th path of the i-th UE, let us define the equivalent angular domain channel vector and matrix for communication and radar channels by $\mathbf{h}_{i,p}^{\rm A} \triangleq \mathbf{F}_{N_{\rm BS}}^{\rm H}\mathbf{a}\left(\varphi_{i,p}\right)$ and $\tilde{\mathbf{H}}_{i,p}^{\rm A} \triangleq \mathbf{F}_{N_{\rm BS}}^{\rm H}\mathbf{A}\left(\varphi_{i,p}\right)\mathbf{F}_{N_{\rm BS}}$, respectively. In particular, we refer to both $h_{i,p}^{\rm A}\left[n_{\rm t}\right]$ and $\tilde{H}_{i,p}^{\rm A}\left[n_{\rm t}, n_{\rm r}\right]$ as the angular domain channel coefficients associated to the p-th path of i-th UE for the $n_{\rm t}$-th transmit antenna of communication and for the $(n_{\rm t}, n_{\rm r})$-th antenna pair of radar, respectively. According to their definitions, we notice that if the value of $\sin\varphi_{i,p}$ is integer multiples of $2/N_{\rm BS}$, the values of $h_{i,p}^{\rm A}\left[n_{\rm t}\right]$ and $\tilde{H}_{i,p}^{\rm A}\left[n_{\rm t}, n_{\rm r}\right]$ will be either one or zero. Therefore, let us define the **angular resolution**[3] by $2/N_{\rm BS}$. According to the angular resolution, we further define the **transmit angular index** by $a_{i,p} \triangleq \left[N_{\rm BS} - \frac{\sin(\varphi_{i,p})N_{\rm BS}}{2}\right]_{N_{\rm BS}} + 1$ and the **receive angular index** by $\tilde{a}_{i,p} \triangleq \left[N_{\rm BS} + \frac{\sin(\varphi_{i,p})N_{\rm BS}}{2}\right]_{N_{\rm BS}} + 1$.

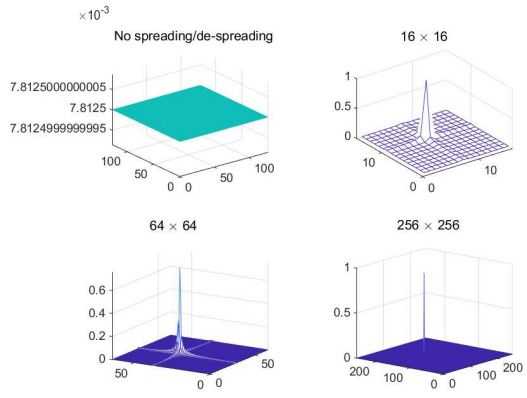

Fig. 3. An illustration of the absolute values of $\tilde{\mathbf{H}}_{i,p}^{\rm A}$ with spatially-spreading/de-spreading, where the angle is $\varphi = \pi/3$.

Remark 2: We notice that the equivalent angular domain channel is sparse when $\sin\varphi_{i,p}$ is integer multiples of $2/N_{\rm BS}$, which can be asymptotically achieved given a sufficiently large number of antennas at the BS. In this case, both $a_{i,p}$ and $\tilde{a}_{i,p}$ are of integer values and we have $h_{i,p}^{\rm A}\left[n_{\rm t}\right] = 0$, for $n_{\rm t} \neq a_{i,p}$, while $h_{i,p}^{\rm A}\left[n_{\rm t}\right] = 1$, for $n_{\rm t} = a_{i,p}$. Furthermore, we have $\tilde{H}_{i,p}^{\rm A}\left[n_{\rm t}, n_{\rm r}\right] = 0$, for $n_{\rm t} \neq a_{i,p}, n_{\rm r} \neq \tilde{a}_{i,p}$, while $\tilde{H}_{i,p}^{\rm A}\left[n_{\rm t}, n_{\rm r}\right] = 1$, for $n_{\rm t} = a_{i,p}, n_{\rm r} = \tilde{a}_{i,p}$.

We demonstrate the effect of spatially-spreading/de-spreading for $\tilde{\mathbf{H}}_{i,p}^{\rm A}$ with a specific angle value $\varphi = \pi/3$ in Fig. 3, where $N_{\rm BS} = 16$, 64, and 256, are considered. As shown in the figure, the angular domain channel response becomes more concentrated with more antennas. Although the integer transmit and receive angular indices may only exist with a sufficiently large number of antennas, it can be shown that the closest integer numbers to $a_{i,p}$ and $\tilde{a}_{i,p}$ will have the strongest angular response in the fraction case. According to the above discussion, it is natural to design the indicator matrices $\mathbf{P}_1$ and $\mathbf{P}_2$ such that the TDS domain transmitted and received symbol vectors are aligned with $a_{i,p}$ and $\tilde{a}_{i,p}$, respectively. In this case, the DD domain received symbol vector can be written by

$$\mathbf{y}_i = \sum_{p=1}^{P} h_{i,p}^{\rm A}\left[a_{i,p}\right] \mathbf{H}_{i,p}^{\rm DD} \mathbf{x}_i + \mathbf{w}_i. \quad (8)$$

where $\mathbf{H}_{i,p}^{\rm DD} \triangleq \left(\mathbf{F}_N \otimes \mathbf{I}_M\right)\mathbf{H}_{i,p}^{\rm TD}\left(\mathbf{F}_N^{\rm H} \otimes \mathbf{I}_M\right)$ is the effective D-D domain channel matrix and $\mathbf{w}_i$ is the equivalent noise term consisting of the noise and possible interferences from multi-user transmission. Similar to (8), the TDA domain radar received sym-

[2]Since the UE only has one antenna, the spatial/angular domain features from the receiver side, e.g., receiver steering vector, are disappeared. Therefore, we use the term TD instead of TDS/TDA for the relevant descriptions for the communication receiver in sequel.

[3]It should be noted that due to the nonlinearity of the sin function, it is difficult to define the resolution in the actual angular domain. Here, the resolution is defined with respect to the sin values of the angles.

bol matrix on the i-th RF chain can be written by

$$\tilde{\mathbf{v}}_i = \tilde{H}_{i,2}^{\mathrm{A}} \left[a_{i,2}, \tilde{a}_{i,2}\right] \tilde{\mathbf{H}}_{i,2}^{\mathrm{TD}} \mathbf{v}_i + \tilde{\mathbf{w}}_i, \tag{9}$$

where $\tilde{\mathbf{w}}_i$ is the equivalent noise term consisting of the noise and possible interferences to the i-th RF chain. Other than the SINR, beampattern is also a common radar performance matric. According the transmitted symbol matrix in (3), we can define the beampattern [16] by

$$P\left(\varphi\right) \triangleq \mathbf{a}^{\mathrm{H}}\left(\varphi\right) \tilde{\mathbf{F}}_1^{\mathrm{H}} \tilde{\mathbf{F}}_1 \mathbf{a}\left(\varphi\right). \tag{10}$$

respectively.

4. NUMERICAL RESULTS

In this section, we evaluate the performance of SS-OTFS-enabled ISAC transmission in terms of the communication and radar SINRs, and the radar beampattern. Without loss of generality, we set $K = 8$ and $P = 3$, respectively. We are interested in the SINR comparisons between the proposed scheme and conventional beamforimg-based benchmark, where the beamforimg-based approach applies the same OTFS modulation structure and generates the transmit and receive beamformer based on the corresponding steering vectors. Without loss of generality, we set $M = 16$, $N = 8$, and the AoDs are uniformly generated from $[-\pi/2, \pi/2]$, while the delay and Doppler indices are uniformly taking values from $[0, 3]$ and $[-4, 4]$, respectively. Furthermore, we assume that both the communication and radar channel responses follow an exponential power delay profile with an exponent -0.5 [17].

Fig. 4 provides the communication SINR performances of the proposed scheme with both integer and fractional angular indices for various numbers of antennas, where accurate *a priori* information on AoDs is assumed and the average signal-to-noise ratio (SNR) on each antenna for transmission is 20 dB. As shown in the figure, the proposed scheme has a better SINR performance for communication compared to the beamforming benchmark even in the case of fractional angular index. This indicates that spatially-spreading generally enables a better beam separation compared to the beamforming. Furthermore, with an increased number of antennas, the SINR of the fractional case approaches the ideal integer case, where the inter-beam interference is perfectly cancelled by spatially-spreading. This is due to the fact that the angular resolution improves with more antennas.

The radar SINR performances of the proposed scheme with various numbers of antennas are shown in Fig. 5(a), where the average SNR on each antenna for transmission is 10 dB. As a benchmark, we consider an beamforming-based transmission, where both transmit and receive beamforming are performed for radar sensing in order to distinguish the received echoes from different UEs. We also present the SINR results with AoD errors, where the error (in degree) to each AoD estimate is assumed to have a uniform distribution within $[-2, 2]$. As can be observed from the figure, the SINR performance of the proposed scheme with integer angular indices and accurate AoDs is almost constant with different number of antennas at the BS, which is due to the perfect beam separation in the integer case. Furthermore, we notice that in the case of fractional angular indices with accurate AoDs, the beamforming scheme has a better SINR performance than the proposed scheme. This is because the AoDs are perfectly known at the BS, and therefore, the receive beamforming can significantly improve the SINR performance. On the other hand, we notice that the proposed scheme outperforms the beamforming counterpart in the case of fractional indices with AoD errors, which implies that spatial spareading/despreading generally enables a higher tolerance of the angle estimate error. This is not unexpected because the effects of fractional indices and AoD errors may cancel out with each other and thus, it may still have a strong response as long as the actual AoD value is close to the corresponding angular grid point. We demonstrate the beampattern analysis for $N_{\mathrm{BS}} = 32$ antennas in Fig. 5 (b), where there are in total four paths with AoDs given by $[-60°, -30°, 30°, 45°]$. In particular, it can be shown that the AoDs with $\pm 30°$ correspond to integer indices, while the other two AoDs correspond to fractional indices. We can observe from the figure that the AoDs with integer indices are having the maximum beam gain, while the beam gains for AoDs with fractional indices are smaller, which is the cost of sending orthogonal beams. However, it should be noted that this beam gain loss is not much given a sufficient number of antennas.

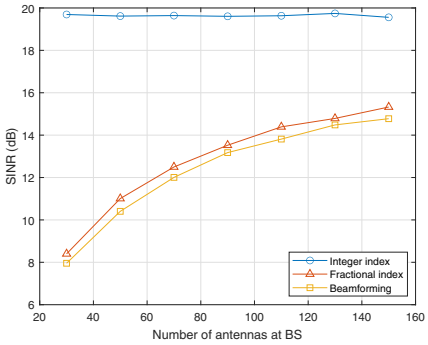

Fig. 4. Communication SINR comparisons between the proposed scheme and beamforming-based approach.

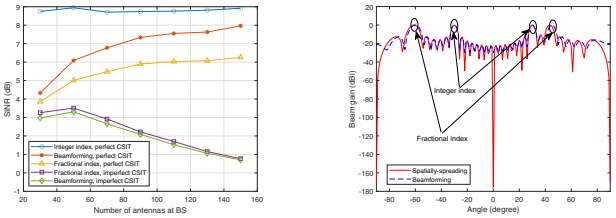

(a) Radar SINR comparisons. (b) Beampattern analysis.

Fig. 5. Simulations of radar SINR and radar beampattern.

5. CONCLUSIONS

In this paper, we studied the potentials of SS-OTFS for ISAC transmissions. We first derived the input-output relationships for SS-OTFS-enabled ISAC system in a typical downlink MU-MIMO scenario. Then, we analyzed the angular domain channel features and presented some discussions on the system design. Finally, our numerical results demonstrated the advantages of the proposed scheme over the conventional beamforming counterpart in terms of the SINR.

6. REFERENCES

[1] Fan Liu, Christos Masouros, Athina P Petropulu, Hugh Griffiths, and Lajos Hanzo, "Joint radar and communication design: Applications, state-of-the-art, and the road ahead," *IEEE Trans. Commun.*, vol. 68, no. 6, pp. 3834–3862, Jun. 2020.

[2] Weijie Yuan, Zhiqiang Wei, Shuangyang Li, Jinhong Yuan, and Derrick Wing Kwan Ng, "Integrated sensing and communication-assisted orthogonal time frequency space transmission for vehicular networks," to appear in *IEEE J. Sel. Topics. Signal Process.*, 2021.

[3] Fan Liu, Christos Masouros, Ang Li, Huafei Sun, and Lajos Hanzo, "MU-MIMO communications with MIMO radar: From co-existence to joint transmission," *IEEE Trans. Wireless Commun.*, vol. 17, no. 4, pp. 2755–2770, Apr. 2018.

[4] Mari Kobayashi, Giuseppe Caire, and Gerhard Kramer, "Joint state sensing and communication: Optimal tradeoff for a memoryless case," in *IEEE Int. Symp. Inf. Theory (ISIT)*, 2018, pp. 111–115.

[5] R. Hadani, S. Rakib, M. Tsatsanis, A. Monk, A. J. Goldsmith, A. F. Molisch, and R. Calderbank, "Orthogonal time frequency space modulation," in *Proc. 2017 IEEE Wireless Commun. Net. Conf. (WCNC)*, 2017, pp. 1–6.

[6] Shuangyang Li, Jinhong Yuan, Weijie Yuan, Zhiqiang Wei, Baoming Bai, and Derrick Wing Kwan Ng, "Performance analysis of coded OTFS systems over high-mobility channels," to appear in *IEEE Trans. Wireless Commun.*, 2021.

[7] Zhiqiang Wei, Weijie Yuan, Shuangyang Li, Jinhong Yuan, Ganesh Bharatula, Ronny Hadani, and Lajos Hanzo, "Orthogonal time-frequency space modulation: A promising next-generation waveform," *IEEE Wireless Commun.*, vol. 28, no. 4, pp. 136–144, Aug. 2021.

[8] Shuangyang Li, Weijie Yuan, Zhiqiang Wei, and Jinhong Yuan, "Cross domain iterative detection for orthogonal time frequency space modulation," to appear in *IEEE Trans. Wireless Commun.*, 2021.

[9] Patchava Raviteja, Khoa T Phan, Yi Hong, and Emanuele Viterbo, "Orthogonal time frequency space (OTFS) modulation based radar system," in *IEEE Radar Conf. (RadarConf)*, 2019, pp. 1–6.

[10] Lorenzo Gaudio, Mari Kobayashi, Giuseppe Caire, and Giulio Colavolpe, "On the effectiveness of OTFS for joint radar parameter estimation and communication," *IEEE Trans. Wireless Commun.*, vol. 19, no. 9, pp. 5951–5965, Jun. 2020.

[11] Lorenzo Gaudio, Mari Kobayashi, Giuseppe Caire, and Giulio Colavolpe, "Hybrid digital-analog beamforming and MIMO radar with OTFS modulation," *arXiv preprint arXiv:2009.08785*, 2020.

[12] Chang Liu, Weijie Yuan, Shuangyang Li, Xuemeng Liu, Derrick Wing Kwan Ng, and Yonghui Li, "Learning-based predictive beamforming for integrated sensing and communication in vehicular networks," *arXiv preprint arXiv:2108.11540*, 2021.

[13] Shuangyang Li, Weijie Yuan, Chang Liu, Zhiqiang Wei, Jinhong Yuan, Baoming Bai, and Derrick Wing Kwan Ng, "A novel ISAC transmission framework based on spatially-spread orthogonal time frequency space modulation," to appear in *IEEE J. Sel. Areas Commun.*, 2022.

[14] P. Raviteja, Y. Hong, E. Viterbo, and E. Biglieri, "Practical pulse-shaping waveforms for reduced-cyclic-prefix OTFS," *IEEE Trans. Veh. Technol.*, vol. 68, no. 1, pp. 957–961, Jan. 2019.

[15] Sudhir Shrestha, Mercyma Deeba Balachandran, Mangilal Agarwal, Li-He Zou, and Kody Varahramyan, "A method to measure radar cross section parameters of antennas," *IEEE Trans. Antennas Propag.*, vol. 56, no. 11, pp. 3494–3500, Nov. 2008.

[16] Daniel R. Fuhrmann and Geoffrey San Antonio, "Transmit beamforming for MIMO radar systems using signal cross-correlation," *IEEE Trans. Aerosp. Electron. Syst.*, vol. 44, no. 1, pp. 171–186, Jan. 2008.

[17] Shuangyang Li, Weijie Yuan, Zhiqiang Wei, Jinhong Yuan, Baoming Bai, Derrick Wing Kwan Ng, and Yixuan Xie, "Hybrid MAP and PIC detection for OTFS modulation," to appear in *IEEE Trans. Veh. Technol.*, 2021.